UC Davis
UC Davis Previously Published Works

Title

The role of site effects on elevated seismic demands and corollary structural damage during the October 30, 2020, M7.0 Samos Island (Aegean Sea) Earthquake

Permalink

https://escholarship.org/uc/item/68w316st

Journal

Bulletin of Earthquake Engineering, 20(14)

ISSN

1570-761X

Authors

Cetin, Kemal Onder
Papadimitriou, Achilleas G
Altun, Selim
et al.

Publication Date

2022-11-01

DOI

10.1007/s10518-021-01265-z

Peer reviewed

The role of site effects on elevated seismic demands and corollary structural damage during the October 30, 2020, M7.0 Samos Island (Aegean Sea) Earthquake

Kemal Onder Cetin, et al. *[full author details at the end of the article]*

Abstract

On October 30, 2020 14:51 (UTC), a moment magnitude (M) 7.0 (USGS, EMSC) earthquake occurred in the Aegean Sea. This paper presents the reconnaissance findings regarding the site effects on recorded strong ground motion intensities and duration, along with the resulting induced-structural damage in Izmir Bay and Samos Island, respectively. In all rock records, relatively high intensity long period rock spectral accelerations were observed in the mid to long period range of 0.5–1.5 s, which are attributed to the source, more specifically, to the slower rupture-mechanism of the event. These rich spectral intensities were further amplified by soil site effects and soil-superstructure resonance, leading to two to six times amplified overall responses and prolonged seismic shaking durations, more pronounced in Bayrakli and other Izmir Bay sites in Turkey. However, these amplified and prolonged excitations are still below design basis earthquake levels, which addresses the lack of proper structural design and construction deficiencies, as the underlying causes for the collapse to heavy damage performance of 795 buildings. On the other hand, although located only about 10 km from the rupture (22 km from the epicenter) and within the near fault zone, the town of Vathy on Samos Island (Greece) was rather lightly affected by the earthquake, with relatively few collapsed or heavily damaged buildings, partially attributed to the low height/low weight of structures in the area. However, a concentration of damage in low-rise buildings in Ano Vathy hill is considered indicative of a combination of coupled valley and topography effects on the strong motion. This event once again addressed the need to develop region-specific zonation and provisions, when more general code practices are proven to be inadequate to assess these extreme site effects.

Keywords Reconnaissance · Samos Island Earthquake · Izmir Bay · Bayrakli · Vathy · Site effects · Amplifications · Resonance

1 Introduction

On October 30, 2020 14:51 (UTC), a moment magnitude (M) of 7.0 earthquake occurred in the Aegean Sea. The epicenter of the event (N 37.8881°, E 26.7770°) is approximately 10 km north of Avlakia-Samos Island, and 23 km south of Doganbey-Izmir, with a focal

Fig. 1 Eastern part of Izmir Bay showing densely populated and highly-affected districts and the location of strong ground motion stations

depth of 17.26 km (AFAD, Disaster and Emergency Management Presidency; www.afad. gov.tr). The Samos (Aegean Sea) earthquake is noteworthy to discuss due to: (1) heavily damaged 7–9 story residential structures concentrated in Bayrakli district of Izmir Bay, which is located approximately 70 km north-east from the epicenter, relatively far away from the fault rupture; (2) relatively few collapsed or heavily damaged buildings in Vathy (Samos Island), despite its proximity to the fault rupture (~ 10 km). Structural damages in Vathy are concentrated on zones, where combined valley and topographic effects are more pronounced. This paper presents reconnaissance findings regarding the role of site effects on locally-concentrated structural damages.

2 Izmir Bay

The city of Izmir is located around the inner Izmir Bay (Fig. 1) in Turkey. Northern, eastern and southern coasts of Inner Izmir Bay are the most densely populated areas of the city of Izmir. All these coastal areas are founded on deep alluvial sediments.

Although located at about 65–70 km to the N–NE of the earthquake epicenter, the city of Izmir was rather unexpectedly and relatively heavily affected by the earthquake. Figure 2 shows the location of moderate to heavily damaged buildings, mostly concentrated in Bayrakli district of Izmir Bay. Compared to the overall building stock (approximately 670,000 buildings; 88.5% residential and 11.5% non-residential) in Izmir Bay, approximately 800 buildings either collapsed or were heavily damaged during this event. Sadly, most of the 118 total life losses (116 in Turkey and 2 in Samos Island) were due to residential building collapses in Izmir-Bayrakli, one of which will be illustratively shown later in Fig. 15.

As an interim remark, which will be discussed in more detail later in the manuscript, when strong ground motion records from Izmir Bay are studied, the ones from soil sites are observed to have significantly larger intensities (0.05 g $< PGA_{soil} < 0.15$ g) as compared to those from rock sites (0.03 g $< PGA_{rock} < 0.06$ g), clearly revealing pronounced site amplifications, reaching to a factor of 2–4 from peak ground acceleration point of view. Significant differences in the frequency content, as well as in the duration of the records, are also observed. The differences are mostly attributed to the variability in geological, morphological, and geotechnical settings of the regions, which will be briefly discussed next.
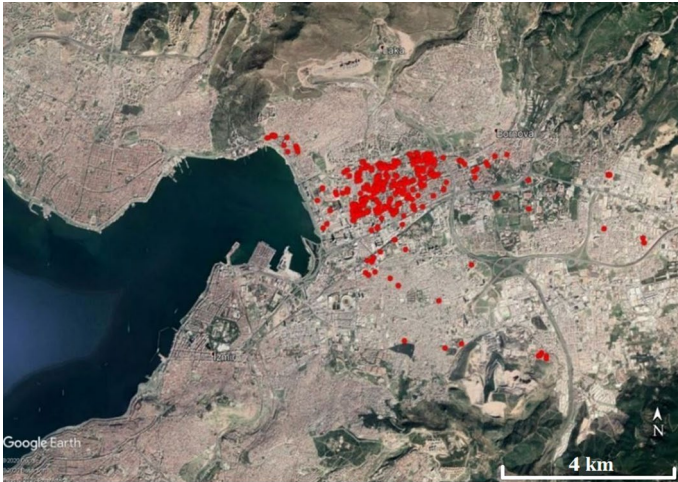
Fig. 2 The scatter of moderate to heavily damaged structures in the east of Izmir Bay (Bayrakli)

## 2.1 Geological, morphological and geotechnical settings of Izmir Bay

The Bornova Melange is the basement in and around the Izmir city (Erdoğan 1990; Koca 1995; Kıncal 2005). It is made up of sandstone–shale intercalations bearing limestone lenses and blocks of limestone, serpentinite, and mafic volcanic rock. Neogene age sedimentary rocks discordantly overlie the Bornova melange consisting of conglomerate, sandstone, mudstone, siltstone, and limestone lithologies. Yunt Mountain volcanic rocks are widespread in and around the northern part of Izmir Bay. The Upper Miocene volcanic rocks, which lie on top of the Neogene aged sedimentary rocks were formed by several volcanic activities in the region. The majority of Karsiyaka and Cigli districts is located on a typical alluvial delta in front of the Yamanlar Mountain blocks. The old Gediz River Delta, which is in the north-western part of Karsiyaka and Bostanli districts, was formed by sedimentation of alluvial deposits transported by the Gediz River in the Quaternary Era.

As shown in Fig. 3, Bayrakli, the most affected district from the earthquake, is located on a very deep alluvial basin, which is bordered to the north and south by hills. While most of the district is founded on quaternary alluvial sediments of the basin, the outskirts extend over the rising slopes of the rock outcrop to the north and south. The bedrock of north side descends, tending south, and reaches a depth of about 1000 m beneath the alluvium underlying the Bayrakli district. The composition and characteristics of alluvium are spatially variable in horizontal and vertical directions. The detailed geological and geophysical investigations conducted in the Bayrakli district revealed the underground soil and rock characteristics as illustrated in Figs. 3 and 4.

The basins of Bayrakli and Bornova districts are bordered to the north and south by active E-W extending normal faults, as shown with red lines in Fig. 1. The young (Holocene) alluvium, several river delta, and shallow marine deposits are confined by Izmir Fault in the South, and Karsiyaka-Bornova fault in the North. As illustrated in Fig. 4, it constitutes the uppermost soft sediments in the basin, reaching 300 m depth by the inner bay. The groundwater table is located at a maximum of 5 m depth in the vicinity of the shoreline.
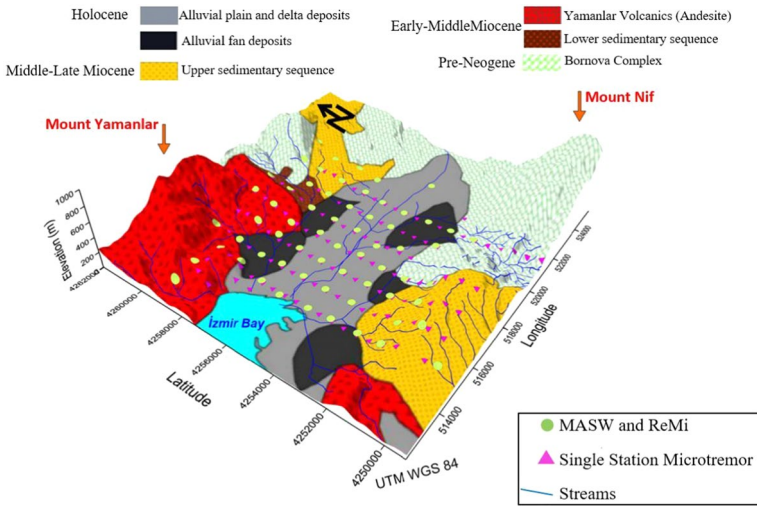
Fig. 3 Geological map of the study area indicating the location of geophysical studies performed in Bayrakli and Bornova districts (After Pamuk et al. 2019)
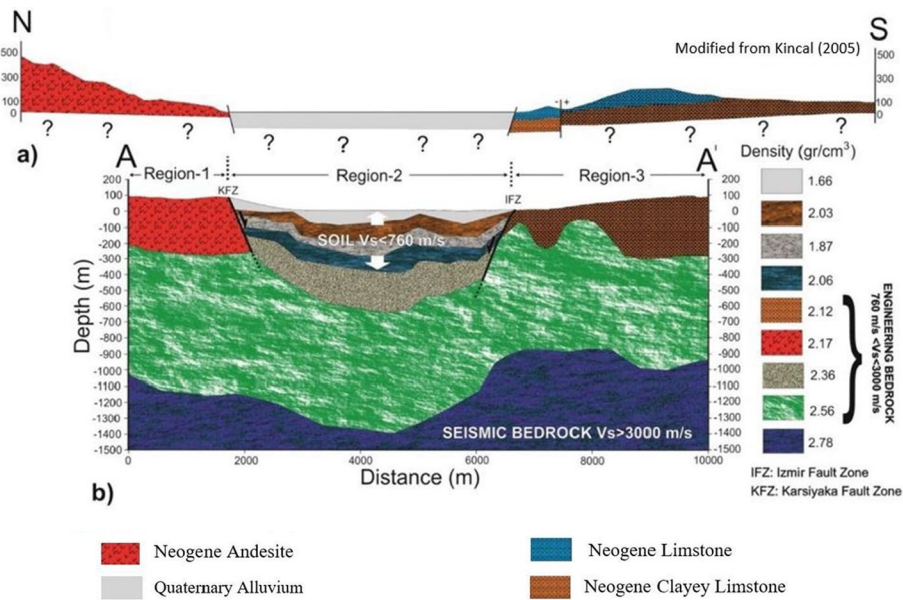
Fig. 4 Geological cross-section of the Inner Izmir Bay developed based on geophysical measurements (After Pamuk et al. 2017)

The very soft sediments and basin edge geometry and structure played a significant role in amplifying the ground shaking.

For the purpose of illustrating the differences in local soil site conditions in Izmir, Fig. 5 is prepared, which presents typical borelogs, compiled from selected residential districts.
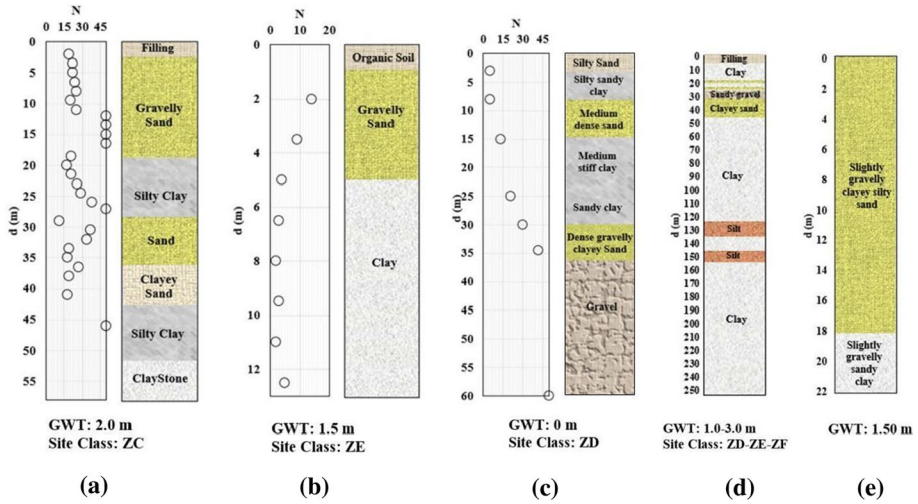
Fig. 5 Typical borelogs from selected residential districts. **a** Gumuldur (after DTA Proje, Personnel communication, 2020), **b** Sigacik-Seferihisar (after Akbuga 2019), **c** Mavisehir (after Kubilay 2012) and **d** Bayrakli (after Pamuk et al. 2018a), **e** Karsiyaka Semikler (Ecemis 2020, personal communication)

Deep alluvial soil layers underlie residential structures at Bayrakli, Bornova, Mavisehir, and Karsiyaka Districts located by Izmir Bay. These very deep (> 200 m) soft, mostly low plasticity clayey soil profiles with interbedded silt, sand, and gravel are judged to be the governing factor behind the pronounced site effects.

2.2 Comparative assessment of available rock and soil motions recorded in Izmir Bay

For the purpose of quantitatively assessing the effects of site conditions on strong ground motion characteristics, the response spectra are given in Fig. 6a, b, respectively, for soil and rock sites. The same scale was used in both figures to enable visual comparison between soil and rock spectra. On the same figures, mean and ± 1 standard deviations of recorded ground motions' response spectra values are also shown, which are estimated simply by taking the average of soil or rock spectra. As clearly revealed by these figures, peak ground accelerations at Izmir Bay soil sites vary in the range of 0.05 g–0.15 g, compared to those of rock varying in the range of 0.03 g–0.06 g. This simple comparison revealed that peak ground acceleration intensities are amplified by a factor of 2–4. Similarly, and more importantly, spectral acceleration values at 0.5–1.5 s period range reach 0.4–0.5 g levels at soil sites, compared to 0.1–0.2 g levels at rock sites. When these 4–5 times amplified spectral acceleration values at 0.5–1.5 s period range, are jointly considered with the seismic response of 7–9 story reinforced concrete buildings of Izmir Bay (more specifically Bayrakli) with natural period of 0.9–1.1 s, the resonance of the soil-structure system is inevitable. The concentrated damage on mostly 7–9 story buildings located in the Bayrakli region is attributed to these site effect-induced amplifications and resonance along with other structural engineering factors, which are discussed in the companion manuscript of Yakut et al. (2021).
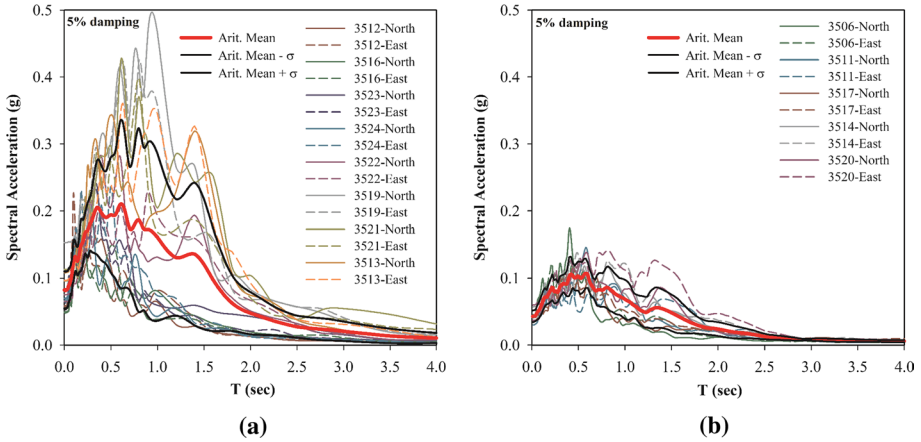
Fig. 6 Elastic response spectra of strong ground motions on **a** soil and **b** rock sites in Izmir Bay
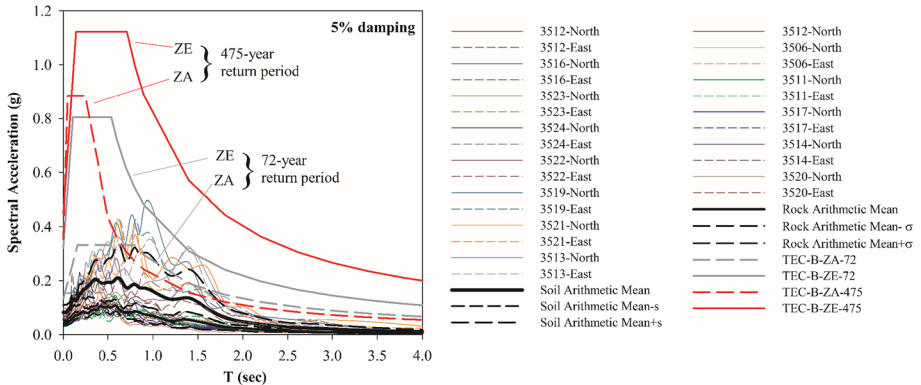
Fig. 7 Comparisons of recorded strong ground motion stations with design basis (475-year return period) and 72-year return period response spectra

With the intent of assessing if the amplified seismic demand levels exceed design basis earthquake intensities, they are comparatively presented in Fig. 7, with those of 72- and 475-year return period events as per Turkish Earthquake Design Code (2018) for soil classes ZA ($V_{s,30} > 1500$ m/s) and ZE ($V_{s,30} < 180$ m/s)). Figure 7 clearly reveals that despite 2–5 times amplifications, the seismic demand in Izmir Bay is observed to be lower than that of design basis level (i.e.: 475-year return period event) and is comparable with a 72-year return period event.

For the purpose of better understanding the site effect-induced amplifications, soil spectral acceleration values were normalized with those of nearest rock sites. Estimated amplification response spectra were plotted as given in Fig. 8. This figure clearly illustrates amplifications reaching a maximum of 6–7 in the east–west direction at Bayrakli station. Again, elevated amplifications at the period range of 0.5–1.5 s are observed. The top three soil sites, where amplifications are observed to be the most pronounced (also the locations where site effects are predominant) are listed as Konak, Karsiyaka, Bayrakli, consistent with the geological, morphological, and geotechnical settings discussed earlier. Among
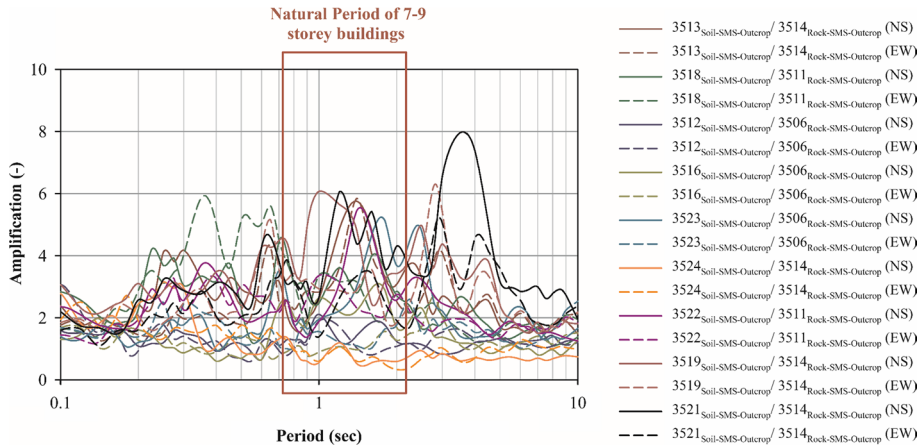
Fig. 8 The amplification spectra, estimated by normalizing the spectral soil accelerations with those of the nearest rock sites

them, the Konak station site is speculated as not being free field due to the presence of an underground parking lot in the immediate vicinity of the station. Hence, its use and interpretation require further careful advance assessments.

2.3 Preliminary site response assessments for Bayrakli Station

With the intent of better understanding these site effects, preliminary 1-D total stress-based equivalent linear site response assessments were performed for Bayrakli station 3513. As shown in Fig. 9, nearby rock motion 3514 was de-convolved to 1500 m depth, where the seismic bedrock was reported to be located (Pamuk et al. 2018b). The representative site profiles shown in Fig. 9 for 3513 (soil site) and 3514 (rock site) were tailored by jointly assessing available shallow and deep borelogs along with available deep V_s profiles. For convenience, the idealized soil profile for station 3513, is trimmed to be extended to approximately 300 m depth, with slight smoothing of stepwise given shear wave velocity profile. A complete documentation of shear wave velocity profiles is presented elsewhere (Cetin et al. 2021), and will not be repeated herein due to page limitations.

More specifically, the soil profile in Bayrakli consists of deep alluvial deposits of alternating thin gravel, silty sand, silty clay, and clay layers, with field (raw) SPT-N values less than 30 blows/30 cm in the upper 200 m. The groundwater table in Bayrakli is located at 1–3 m depth, in the average. As stated earlier, the depth to the engineering bedrock ($V_s > 3000$ m/s) layer is documented to vary in the range of 1100 m to 1200 m (Pamuk et al. 2018b) and may reach up to 1500 m. Modulus degradation and damping relationships of Seed and Idriss (1970), Vucetic and Dobry (1991), Rollins et al. (2020), Schnabel (1973) were used as part of preliminary site response analyses to assess the individual response of sand, low plasticity clay, gravel, and rock layers, respectively. Site-response estimated outcrop response spectra were comparatively shown with those of the recorded, in the upper left corner of Fig. 9. A relatively reasonable match with the recorded motion validated the developed preliminary 1-D model. The amplification response spectra are also shown in Fig. 10, revealing again large amplifications of the within rock motions, reaching as high as 18 at the period range of 0.5–1.5 s.
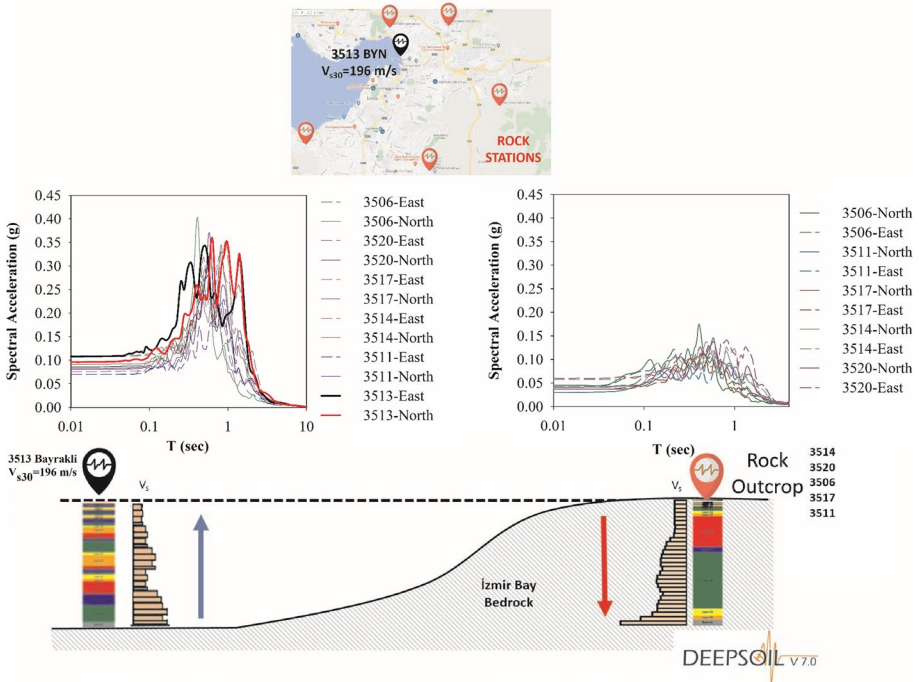
Fig. 9 Preliminary 1-D site response model and analysis results for Bayrakli Station 3513
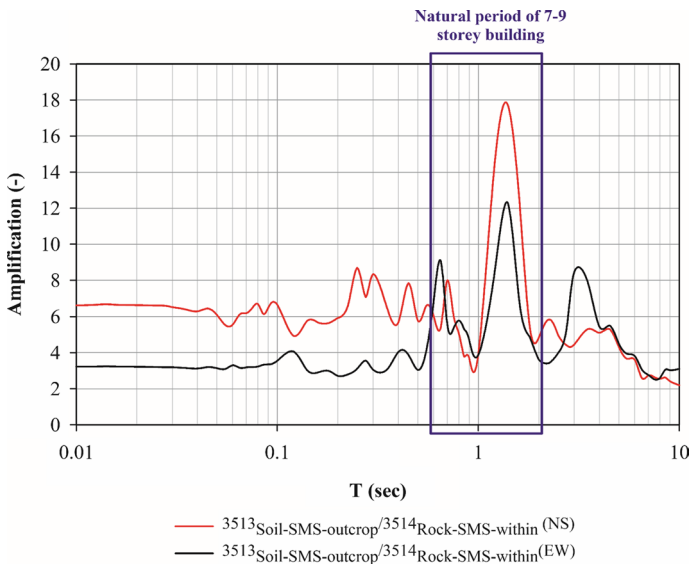

Fig. 10 Amplification spectra estimated by 1-D Site Response Analyses for Bayrakli Station

2.4 Comparisons with code-based amplification factors

The amplification spectra given in Fig. 8 is also compared with the amplification factors presented in Turkish Earthquake Design Code, TEC (2018), as shown in Fig. 11. It should be noted that TEC (2018) suggests similar intensity and site class-dependent amplification factors with those of NEHRP (2020) and Eurocode 8 (2004). It is clearly seen that due to unique soil and site conditions in Izmir Bay, amplifications in excess of code-based recommended values are observed. This observation clearly addresses the need for region-specific seismic zonation for Izmir Bay, and more specifically, for Bayrakli and Karsiyaka districts. It should be noted that occasionally, such region-specific assessments may be needed to overcome the limitations of overly generalized earthquake design codes. A vivid example of such a region, where site effects are similarly and largely pronounced, is Mexico City, which is founded on very deep, soft, high plasticity clays of lake deposit origin (e.g.: Mayoral et al. 2019).

2.5 The effects on observed structural damage in Bayrakli

As discussed earlier, deep to very deep soil sites of Izmir Bay, and more specifically of Bayrakli and Karsiyaka with natural periods varying in the range of 0.5–5 s, amplified the spectral accelerations in the period range of 0.5–1.5 s. The amplification ratios as high as 6–7 were observed at these periods. However, these soil site-specific amplifications were not the only reason behind elevated seismic demands and concentrated structural damage in these deep alluvial soil sites. When response spectra of rock motions of Izmir Bay are compared with ground motion prediction equations (GMPE), one of which is illustrated in Fig. 12, it is clearly seen that relatively mid to long period (0.5–1.5 s) rich spectral energy is present in rock motions. On the basis of these plots, it can be concluded that in this mid
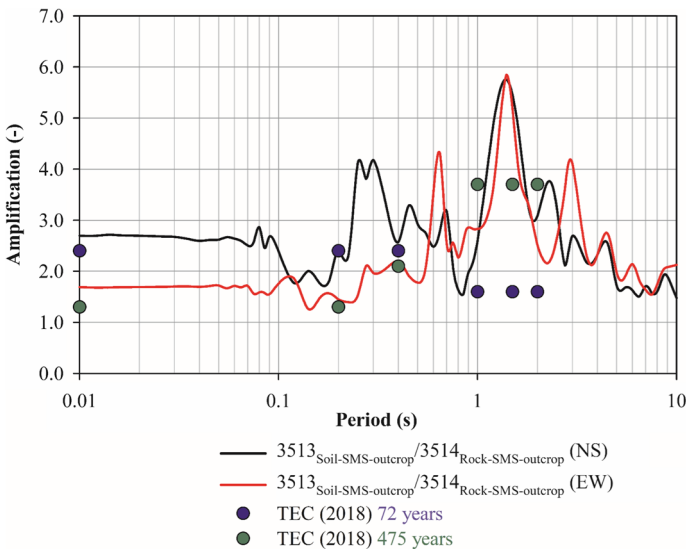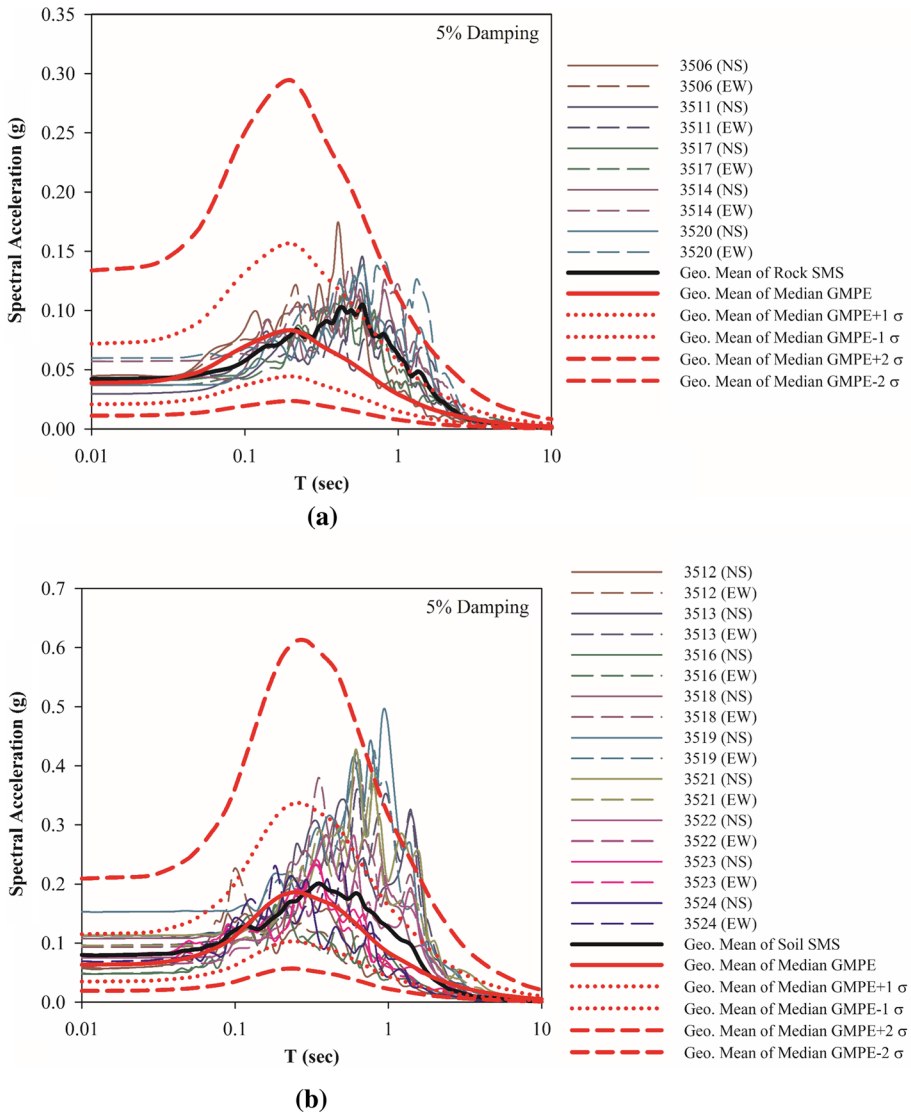

Fig. 11 The amplification spectra for Bayrakli as compared with the amplification factors recommended by TEC (2018)

Fig. 12 The comparison of **a** rock and **b** soil motion response spectra with the predictions of Abrahamson et al. (2014) GMPE

to long period range, the recorded soil and rock spectral acceleration intensities are approximately 2–3 standard deviations above GMPE median predictions. Note that as compared to soil ones, the rock spectral acceleration intensities are also positively biased relative to median predictions. These larger than median GMPE prediction rock intensities are attributed to highly fractured nature of Izmir Bay rock sites due to faulting.

Comparisons of available records with distance attenuations by ground motion prediction equation of Abrahamson et al. (2014), Chiou and Youngs (2014), Campbell and Bozorgnia (2014), Boore et al. (2014), and a detailed compatibility analysis of normalized

residuals decomposed into within-event and between-event components were discussed elsewhere (Gulerce et al. 2021) and will not be repeated herein due to page limitations. Readers are referred to Gulerce et al. (2021) for a more complete discussion.

Moreover, it should be noted that this relatively long period energy is also present in the records closer to the fault rupture, as shown in Fig. 13. Hence, it cannot be attributed to path effects but more to the source mechanism, which leads to richer spectral energy in the period range of 0.5–1.5 s.

As the concluding remark, the bedrock excitation with richer spectral energy at the period range of 0.5–1.5 s due to most likely source effects (more specifically due to relatively slower rupture propagation), is further amplified by the resonating responses of long period, soft, deep soil sites. These already amplified soil outcrop motions were then, once again resonated the 7–9 story residential structures of Bayrakli district. This double resonating system produced largely amplified seismic demands. Moreover, soil site effects were also observed to extend the duration of significant shaking. Figure 14 presents two strong
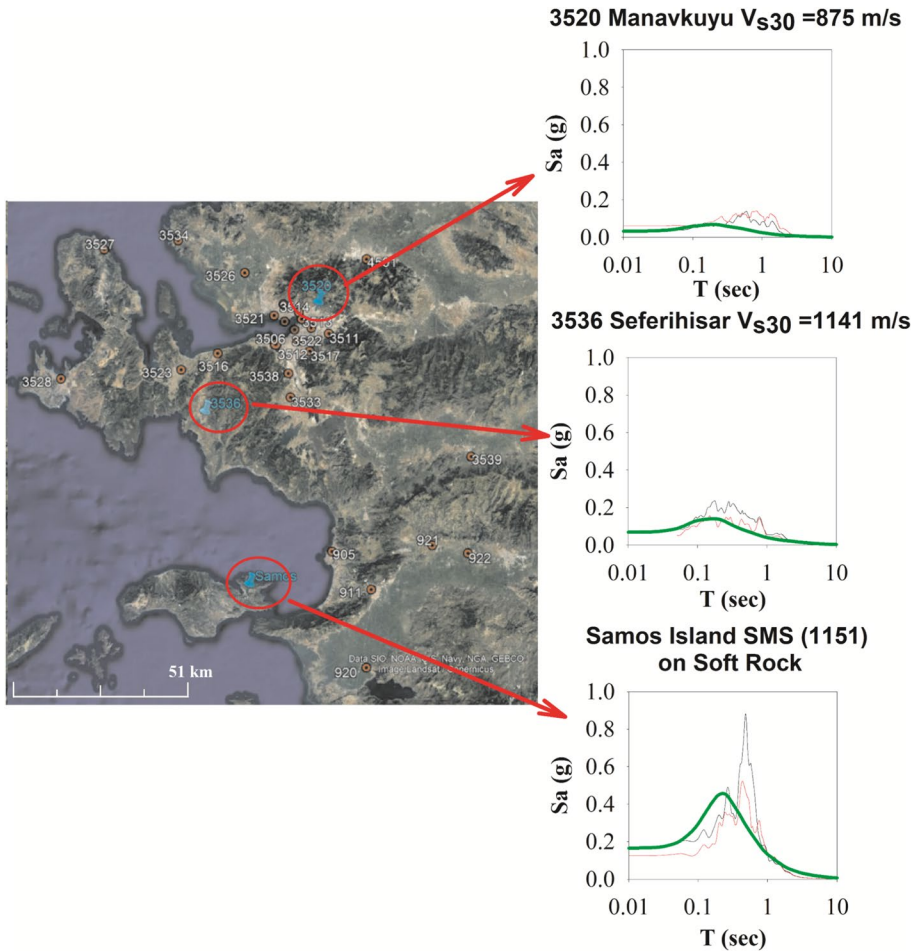
Fig. 13 The response spectra of rock stations closer to fault rupture as compared with the median predictions of Abrahamson et al. (2014)
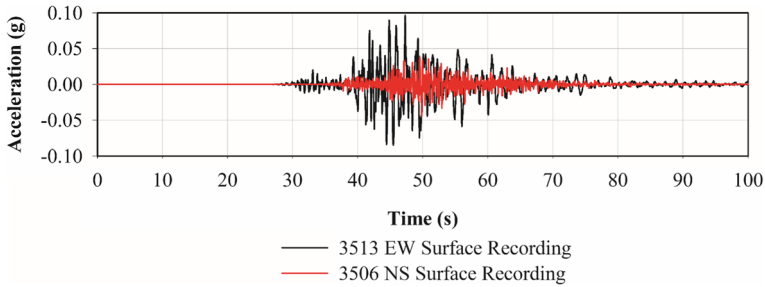
Fig. 14 Two accelerograms obtained at a soil (Bayrakli 3513) and a rock site (Guzelyali 3506) drawn on top of each other to illustrate durational differences

ground motion records obtained at a rock and a soil site, drawn on the same plot to enable visual inspection of durational effects and prolonged coda in the soil record.

However, as stated earlier, these largely amplified and prolonged seismic demands were still below the design basis response spectra. The recent event is not classified as a design basis event, but more of a 72-year return period event. Hence, it is not expected to cause structural damage, not to mention hundreds of collapsed or heavily damaged buildings, one of which is shown in Fig. 15. There, poor structural design and detailing, along with poor construction practices come into the picture, which are discussed in the companion manuscript of Yakut et al. (2021). After having discussed the major reconnaissance findings from the Anatolian (Turkey) side, the discussion will now be directed to Samos Island.

3 Samos Island

The island of Samos (Greece) is situated in the meizoseismal area, right south of the rupture zone, at the footwall of the causative normal fault. Only the northern part of the Island was significantly affected by the earthquake. Except for some coastal areas, the island is covered by stiff soil formations and outcropping rock.

Fig. 15 Doganlar residential building, fully collapsed after the event (courtesy of Ali Aksoyer)

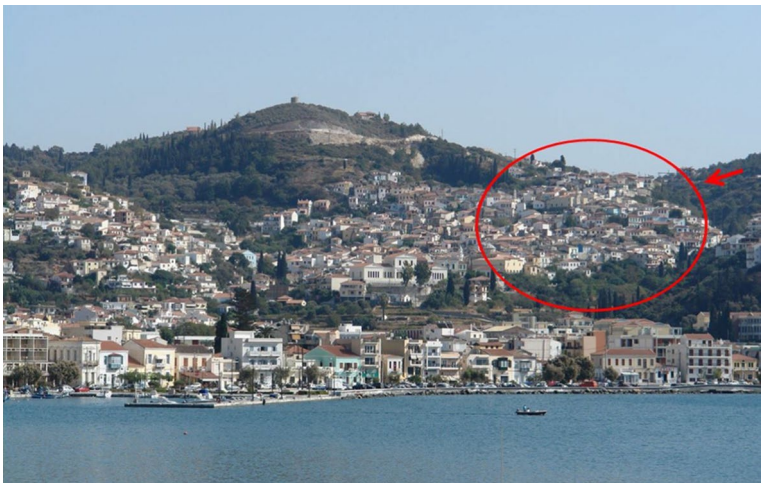**Fig. 16** Town of Vathy, at the north-eastern side of Samos Island

Fig. 17 Ano Vathy hill (at the southeastern side of Vathy) highlighting the area of potential topographic and valley effects (Photo by Christos Giarlelis, HAEE/ETAM Team)

Although located only about 10 km from the ruptured area (22 km away from the epicenter), in the near-fault zone, the seaside town of Vathy (Fig. 16, from Google Earth) at the north-eastern part of the Island was rather lightly affected by the earthquake. Despite the tragic death of 2 high school students in Vathy, the collapsed or heavily damaged buildings were relatively few considering the magnitude of the event and the proximity to the source. Figure 17 shows the area of concentrated damage in the Ano Vathy suburb, which is located up in a hill at the northeastern side of the town of Vathy.

The following three sections briefly discuss the geology of the region, the soil effects related to the two available recordings in Vathy, and the site (i.e., topographic and valley) effects potentially related to the concentrated damage in Ano Vathy hill.

3.1 Geological and geotechnical setting of Samos Island

With reference to the pre-Neogene metamorphic setting, the geological succession on Samos Island consists mainly of four distinct units, as shown in the simplified geological map published by Roche et al. 2019 (Fig. 18). These refer to: (1) the Kerketeas marbles in the western part of the Island, (2) the Ampelos unit, which outcrops over the central part of the Island, (3) the Selçuk nappe, which crops out in the central area of the Island as well, and (4) the Vourliotes nappe which crops out in the eastern part of Samos. More recent Neogene deposits form the Karlovasi and the Mytilini basins, where the dominant geological formations are lacustrine, travertine-like or marly, medium-to-thick limestones and hard marls, with intercalations of clays, sandy marls, breccia with components from the Neogene sediments and conglomerates. Recent Quaternary deposits are mainly present in the Northern-Western and the Southern-Eastern part of the Island, close to the towns of Karlovasi and Pythagorio, respectively. Part of the Samos capital city (Vathy) is also founded in such alluvial sediments, which are composed of clayey-sandy materials, sands and gravels. The detailed geological map of Samos Island published by the Hellenic Survey of Geology and Mineral Exploration (HSGME) is shown in Fig. 19.
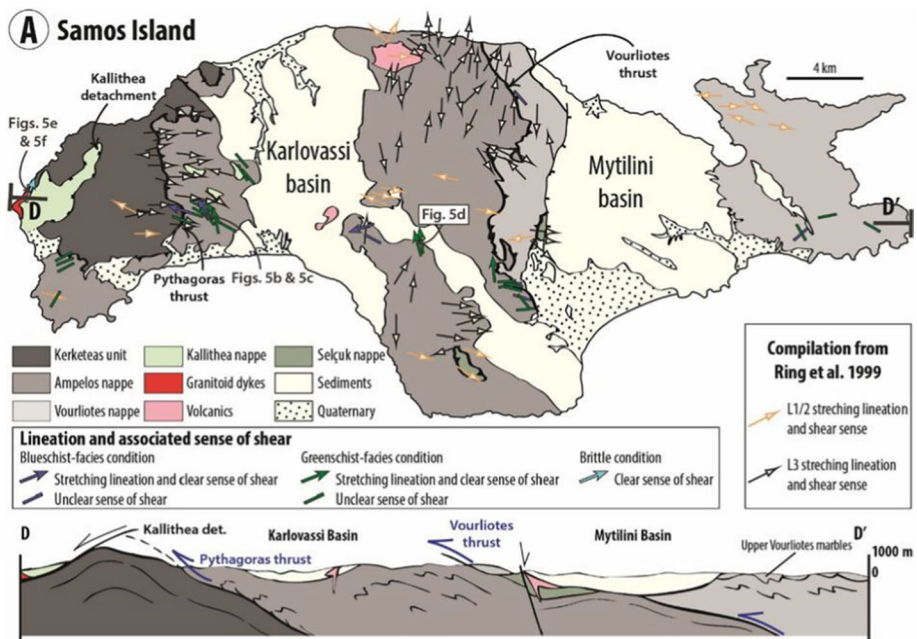
Fig. 18 Simplified geological map of Samos Island, indicating the dominant geological units (Roche et al. 2019)

Fig. 19 Detailed geological map of Samos Island, published by the Hellenic Survey of Geology and Mineral Exploration (HSGME 1979)

Selected sites of the island of Samos are also marked on the geological map in Fig. 19. A short description of the main geological formations in these areas is provided below, given their relevance to the observed damage:

- **Vathy (capital of Samos)** Mainly Quaternary plain deposits of clayey-sandy material, loam, sand and gravels. Such types of recent sediments are also met at the west of Pithagorio on the southern shore and at the north of the Karlovasi basin.

- **Along the Vathy—Karlovasi provincial road** Mainly marly and travertine-like lacustrine limestones with intercalations of low-cohesion marls.

- **Potami (west of Karlovasi)** Dolomitic thin to medium-bedded marbles of Kerketeas unit and schist overlaying Kerketeas marbles.

- **Remataki** Lacustrine, medium-to-thick bedded, travertine-like limestones and thin-bedded marls. The above geological formations dominate the broader area of Pythagorio.

- **Avlakia** Vourliotes marbles with intercalations of schist, and they are met mainly in the eastern side mountainous block of the central island.

Table 1 and Fig. 20 summarize the first collection of geotechnical data with reference to the town of Vathy (the capital of Samos).

3.2 Soil effects at Vathy

The two seismic recordings of the mainshock of the October 30th, 2020 event in Samos Island were acquired within the relatively flat area of the seaside town of Vathy, i.e., near the locations of BH2 and BH3 in Fig. 20. The ITSAK recording was closer to the seafront, while the NOA recording was obtained 235 m to its east, at an elevation 11 m

Table 1 Summary for geotechnical boreholes available in the area of Vathy, location, and source

| BH notation	Site description	Location		Depth (m)	Source
		LAT	LONG		
BH1	Old Port of Vathy	37.757144°	26.970566°	23.2	Milionis G. (Geologist)
BH2	Municipal Cultural Center "Epikourio"	37.753649°	26.979372°	15	Milionis G. (Geologist)
BH3	Municipal Nursing Home (Vathy)	37.753731°	26.978154°	15	Milionis G. (Geologist)
BH4	New Port of Vathy	37.751489°	26.960249°	20	Milionis G. Geologist)
BH5	New Port of Vathy	37.754001°	26.957913°	21	Ministry for the Environment, Physical Planning and Public Works of Greece
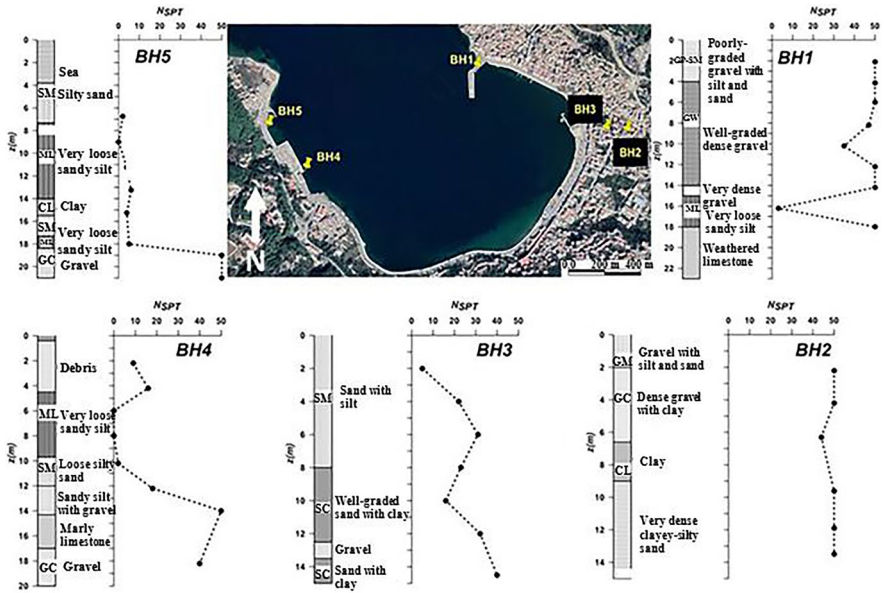
Fig. 20 Selected borehole locations and geotechnical information in the area of Vathy

higher (there is a mild average inclination of 4.5% towards the west, i.e., toward the sea front). Both recordings have been presented in full detail in the respective reports (ITSAK-EPPO 2020, Kalogeras et al. 2020). Of interest here is to combine the information from the recordings with the currently available geological and geotechnical data in an effort to ascertain whether there are any site effects on the recordings. Based on these reports, the recorded motion was more intense in the NE-SW direction of both recording stations, and hence Fig. 21 compares the pertinent acceleration and velocity time-histories at both stations. It shows that the strong ground motion reached PGA and PGV values of 0.23 g and 22 cm/s at the ITSAK station with a strong motion duration of 9 s, whereas the pertinent values of PGA, PGV and duration at the NOA station are equal to 0.17 g, 15 cm/s and 7 s, respectively.

Figure 22 presents a comparative evaluation of the elastic response spectra (5% structural damping) of all (horizontal and vertical) components of acceleration from the two recordings of the October 30th 2020 earthquake at Vathy, i.e., the records from NOA (Kalogeras et al. 2020) and the records from ITSAK (ITSAK-EPPO 2020). The blue curves present the spectral information along the approximately NE-SW direction (see time-histories in Fig. 21), while the red curves refer to the (perpendicular) NW–SE direction. The legends of the various subplots depict the exact orientations of the instruments at the two recording stations.

Particularly, Fig. 22a, b compare the elastic response spectra at the 2 recording stations. It is shown that the main event is characterized by a relatively low-frequency content since at both recordings, the predominant period of the horizontal acceleration is in the order of 0.5 s. This is anticipated given the length of the rupture. Another interesting finding is that the NOA recording is characterized by relatively lower values of spectral acceleration (approximately 20–40% lower for structural periods of practical interest T=0–0.8 s), while the spectral shapes of the two records are quite similar. Given the close proximity
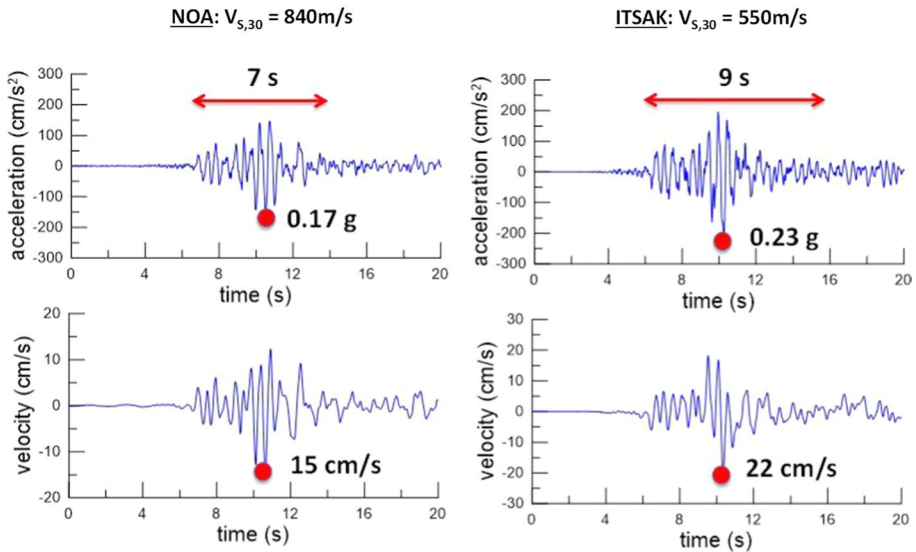
Fig. 21 Comparison of acceleration and velocity time histories of NE-SW records of the October 30th 2020 earthquake at NOA (Kalogeras et al. 2020) and ITSAK (ITSAK-EPPO, 2020) at Vathy

of these stations, compared to the average of about 10 km distance from the rupture zone (epicentral distance of about 22 km), this differentiation is a manifestation of soil effects on the seismic ground motion within the flat area of Vathy. Concurrently, the vertical acceleration has a significantly lower predominant period of 0.1 s and a much smaller amplitude than the horizontal components, without any noteworthy differentiation in the two recording stations. To further explore these findings, Fig. 22c, d compare the horizontal to vertical spectral ratios at the two recording sites. These ratios underline that the NE-SW horizontal components were generally larger than their NW–SE counterparts. They also show predominant peaks at periods around 0.6 s; however, these peaks are significantly more pronounced in the ITSAK recording. Moreover, both recordings depict a similar secondary peak in the large period region (around 1.5 s). Finally, Fig. 22e presents the standard spectral ratio of the two recordings employing the NOA site as the "reference" (bedrock) site. It is deduced that the peak ground acceleration is relatively amplified by 40% on average, higher amplifications appear at intermediate periods 0.1 – 0.6 s, while the amplification diminishes at periods higher than 1 s.

Careful examination of the locations of the two recording sites versus the surface geology in Fig. 23 reveals that the ITSAK recording (Fig. 22b, d) was obtained at an alluvium site closer to the seafront, whereas the NOA recording (Fig. 22a, c) was performed at a location where the marbles outcrop. Obviously, this geological differentiation needs to be verified by a geophysical and geotechnical investigation. This process is ongoing, and the only currently available geotechnical investigations in this particular area of Vathy are two sampling boreholes of 15 m depths, namely BH3 closer to the seafront than the ITSAK recording and BH2 approximately in between the two recording sites, as also shown in Fig. 23. The geotechnical profile with depth (stratigraphy and SPT blow count) of the two boreholes in question is presented in Fig. 24. It is shown that alluvium is found within the first 15 m of both borehole locations (in agreement with the geological map); however, the stiffness of these geomaterials is quite different. In particular, the SPT blow counts are
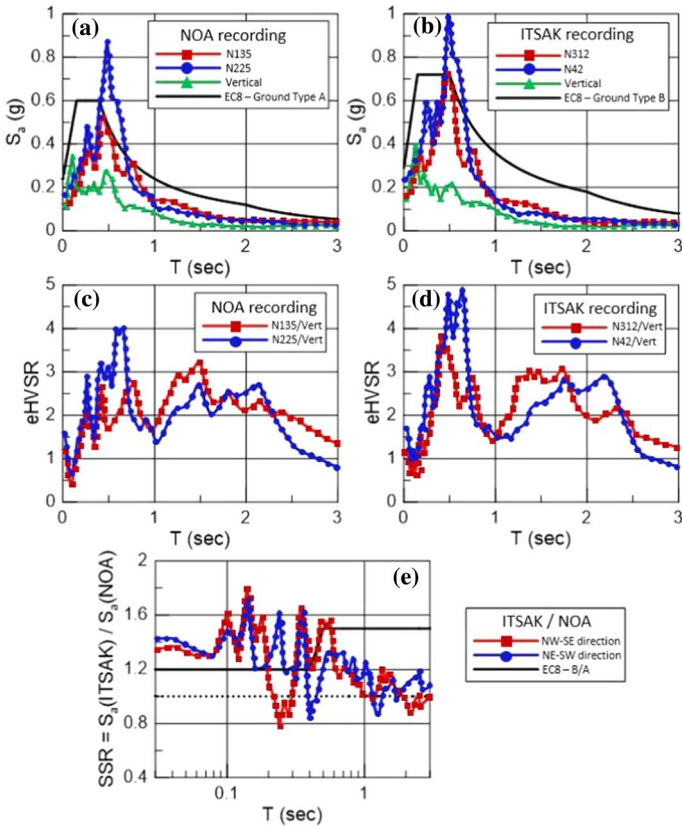
Fig. 22 Comparison of elastic response spectra (5% structural damping) of acceleration records of the October 30th 2020 earthquake at NOA (Kalogeras et al. 2020) and ITSAK (ITSAK-EPPO 2020) at Vathy: **a**, **b** Spectral accelerations; **c**, **d** horizontal to vertical spectral ratios; **e** standard spectral ratios
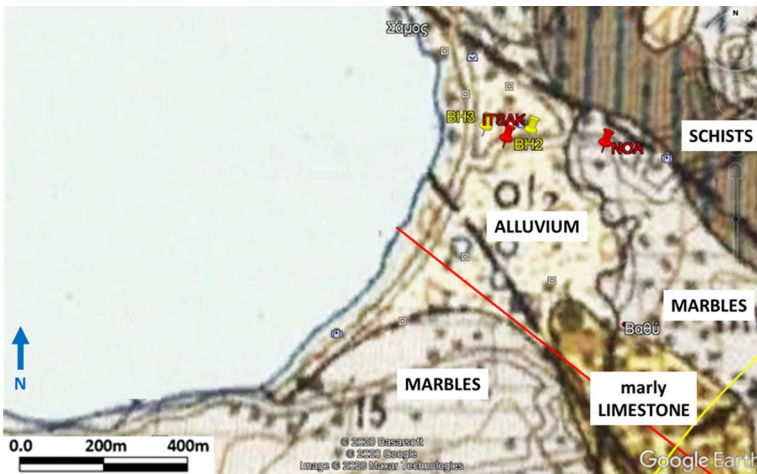
Fig. 23 Detail of geological map of the area of the two recording sites (ITSAK and NOA) at Vathy, as well as locations of two available boreholes (BH3 and BH2); Geological info from HSGME (1979) map
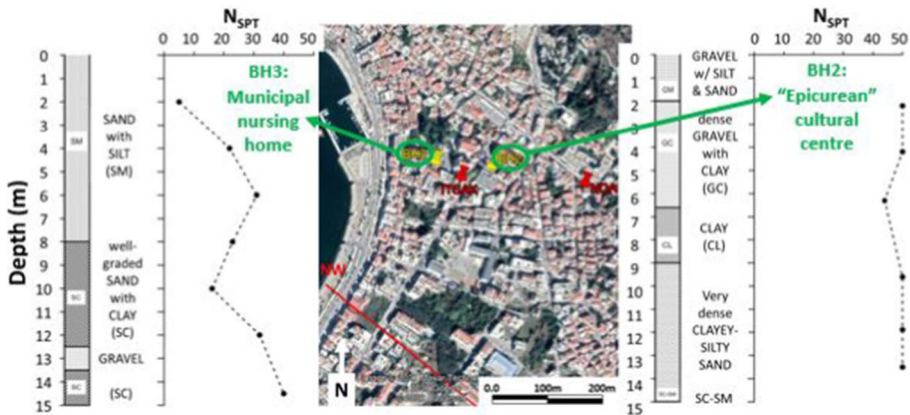
Fig. 24 Geotechnical profile (stratigraphy and SPT blow count) with depth at borehole locations BH2 and BH3 in close proximity of the recording sites (ITSAK and NOA) at Vathy (see also Fig. 22)

well below 45 at the western borehole BH3 (downslope of ITSAK recording site), but are approximately equal to 50 (or more) at all depths in the eastern borehole BH2 (in between the two recording sites). The geological bedrock has not been reached at neither of the two boreholes, since they end at the shallow depth of 15 m. However, it is expected to be shallower in the eastern direction, where the bedrock outcrops (e.g., at the location of the NOA recording).

In closing, one may consider the ITSAK and NOA recording sites as being a "stiff soil" and a "bedrock" site, respectively. This approximation is backed by in-situ geophysical measurements performed by Prof. P. Pelekis (HAEE/ETAM Member and co-author of this paper). These measurements give preliminary estimates of predominant site frequencies (via HVSR microtremor technique) that are well below and above 12 Hz for the ITSAK and NOA recording sites, respectively. These measurements also give preliminary estimates of $V_{s,30}$ (via MASW) at these sites that equal 550 m/s ("stiff soil") and 840 m/s ("bedrock") at the ITSAK and NOA recording sites, respectively. Note that these values are different from preliminary estimates based on proxies developed by Stewart et al. (2014). On the basis of this approximation, the 1D soil amplification (versus the acceleration at outcropping bedrock) is found to be significant within the town of Vathy, i.e., on the order of 30% on average, which is clearly higher than the EC8 soil amplification factor of 1.2 (Ground Category B in EC8 for the ITSAK site, as per the measured $V_{s,30}$ value).

3.3 Basin/topography effects in Ano Vathy

The reconnaissance efforts in the greater area of Vathy depicted a concentration of damage in the low-rise buildings of Ano Vathy hill, an area of about 0.1 km^2 resting in the southeastern side of Vathy (at a distance of 600–1000 m from the coastline), at an elevated location (altitude ranging from 50 to 120 m). The building stock includes several structures dating from the 19th (possibly even the 18th) century, built at a high elevation to protect the inhabitants from pirates. Examples of the observed damage are depicted in Figs. 25 and 26.

Figure 27 shows a Google Earth image of the greater Vathy area, where the suburb of Ano Vathy is depicted by purple shading. This figure also includes two cross-sections: the (red) section having a NW–SE orientation and the (yellow) section with a SW-NE

Fig. 25 Ano Vathy hill: Red circles denote damaged buildings. (Photo by Christos Giarlelis, HAEE/ETAM Team)


Fig. 26 Ano Vathy: Close view of the damaged dome of the Church of Metamorphosi Sotiros and neighboring building. (Photo by Christos Giarlelis, HAEE/ETAM Team)

direction, which will be used to depict the topography of the area in the sequel. The figure also includes with red pins the two recording locations of the mainshock (ITSAK and NOA, with the former being the one closest to the seafront).
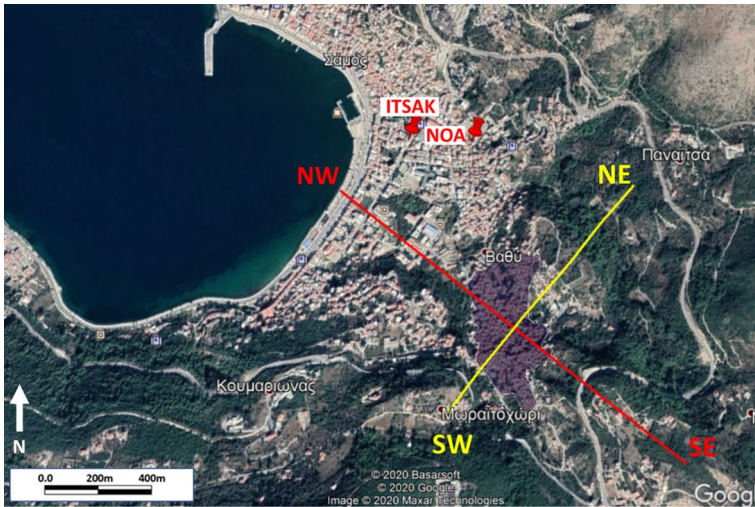
Fig. 27 Location of Ano Vathy (highlighted purple) at the southeastern side of the seaside town of Vathy and depiction of two cross sections and two recording locations of main shock (ITSAK and NOA)

The map of Fig. 28 depicts the geology of the area, with reference to the two afore-mentioned cross-sections. This figure shows that the seafront flat area of Vathy is built on alluvial deposits, namely plain deposits of clayey-sandy material, loam, sand peb-bles, gravels. However, Ano Vathy (the area around the crossing point of the two sec-tions; see Fig. 27) is built mostly on the northern-western end of medium-to-thick bed-ded travertine-like limestones (of probable Miocene age), with intercalations of marls and loose, fine materials, of maximum depth of 80 m. This geological unit lies over the
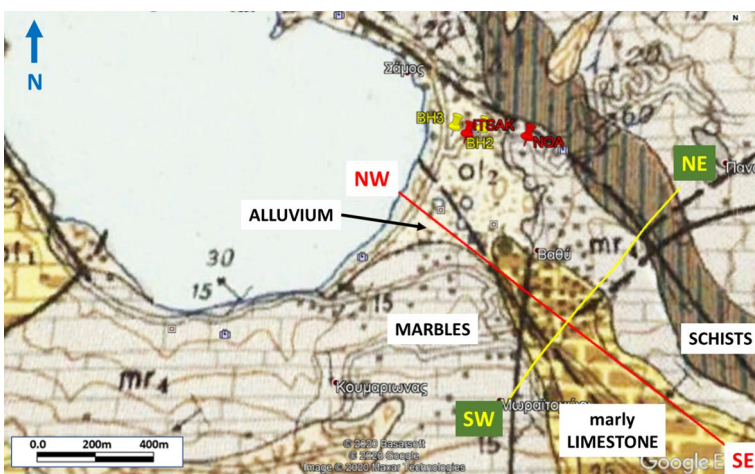
Fig. 28 Geological map of the greater area of the seaside town of Vathy and locations of boreholes (BH2, BH3), recording sites (NOA, ITSAK) in Vathy, as well as NW–SE and SW-NE cross sections running through the damaged area of Ano Vathy; Geological info from HSGME (1979) map

bedrock of the greater area, i.e., medium-to-thick bedded marbles, of a maximum thickness of 500 m, which outcrops towards the SW and NE of Ano Vathy. Of interest is also a probable or covered geologic fault that has an NNW-SSE direction at the western side of Ano Vathy, which may affect the thickness of the marly limestone layer under Ano Vathy. The outcropping limestones at the western part of Vathy gulf, are similar to those of Ano Vathy but of younger (pliocene) age. At the east of Ano Vathy, there is a narrow outcrop of schists (running in parallel to the NW–SE cross section), that surfaces in between marbles, all being metamorphic strata of similarly large stiffness.

Figure 29 shows the ground surface elevation and the (approximate) geological layers that are to be found along the NW–SE section running through the urban area of Ano Vathy. Figure 29a presents the cross-section in natural scale, while Fig. 29b shows the cross-section in distorted scale in order to highlight its details. Hence, subplot b also includes an idealization of the ground surface topography, which shows that the urban area of Ano Vathy is situated at about the mid-height of an H = 170 m tall slope with a mild average inclination angle i = 13°. Geologically, Ano Vathy sits on top of the (marly) limestone formation, which has a thickness ranging approximately from 5 to 30 m along this cross-section and lays over the stiffer bedrock of marbles. The figure also depicts a thick alluvium layer near the seafront, while it includes the projection of the two recording stations (ITSAK, NOA) on the NW–SE section, as well as the location of the second SW-NE section of Fig. 28 that will be studied in the sequel.

Fig. 29 Ground surface elevation and approximate geological cross section along the NW–SE section running through the damaged area of Ano Vathy. Average (idealized) inclination is 13°
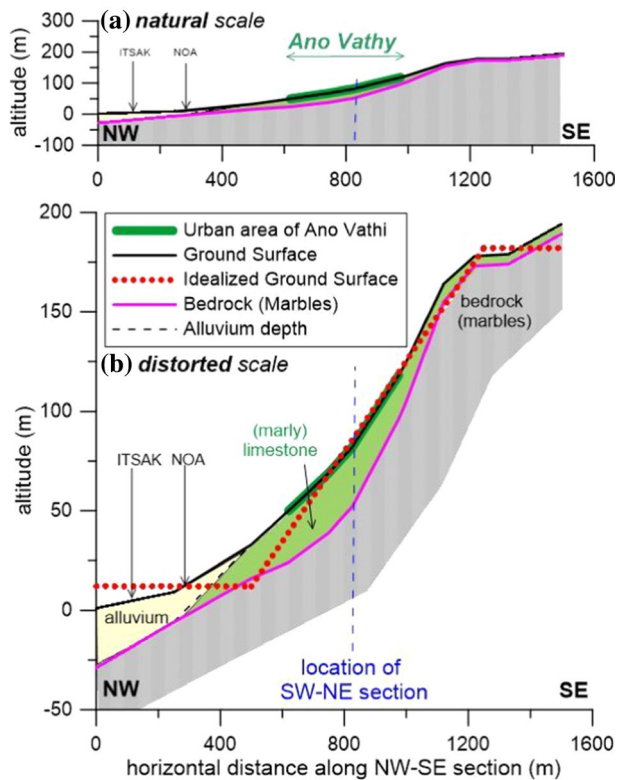
This type of ground surface topography may be marginally considered a cause of increased seismic ground motion at Ano Vathy. Specifically, according to EC8, this is possible for slopes having a height $H > 30$ m, as shown in Fig. 29. However, the same code prescribes that topography effects may be neglected if the inclination angle is $i < 15°$. Disregarding this notion, EC8 also mentions that for ridges with crest width significantly less than the base width, a topography factor $S > 1.2$ should be used near the top of the slopes with angles $i < 30°$ (as this one). Furthermore, this S factor may be assumed to decrease as a linear function of height above the base of the cliff or ridge and to become unity at the base. Hence, for the Ano Vathy area, a factor of $S = 1.1$ may be assumed, as the average of $S = 1.2$ at $H = 170$ m and $S = 1$ at the base, given that it is located at mid-height of the slope.

From another point of view, one may estimate the topographic amplification on the basis of the approximate relations of Bouckovalas and Papadimitriou (2005). Considering the seismic excitation as having a predominant period of $T_e = 0.5$ s (on the basis of the 2 recordings at Vathy; see Fig. 22), and by assuming that the inclined ground has an average shear wave velocity of $V_s = 500$ m/s (near the weathered surface of the marly limestone) to significantly more than 800 m/s (marble bedrock) but a relatively small damping ratio ($\xi = 2\%$), the idealized cross-section with $H = 170$ m and $i = 13°$ shown in Fig. 29 is expected to be characterized by $S = 1.16$ at its crest. Therefore, for the Ano Vathy area that lies at the mid-height of the slope, the $S = 1.08$, on average, which is in good agreement with the EC8 provision. On top of this, Bouckovalas and Papadimitriou (2005) prescribe estimates of a parasitic vertical acceleration due to reflections of incident waves at the non-horizontal ground surface of slopes and the related surface wave generation. The term "parasitic" implies that this component is independent of the incident vertical acceleration of the earthquake and only appears near the slope. As such, its characteristics are a function of the incident horizontal acceleration (intensity, frequency content). For this case, Bouckovalas and Papadimitriou (2005) estimate parasitic vertical acceleration whose peak value is in the order of 14–20% of the peak horizontal acceleration of the earthquake. This vertical acceleration has the low-frequency content of the horizontal motion (predominant period of 0.4–0.6 s; see Fig. 22) and is considered additionally to the vertical acceleration of the earthquake itself, which has a high frequency content (predominant period of 0.1 s; see Fig. 22). This parasitic vertical acceleration is disregarded by EC8.

Figure 30 shows the ground surface elevation as well as the (approximate) geological layers that are to be found along the SW-NE cross-section running through the urban area of Ano Vathy (see location in Fig. 28). Subplot a presents the cross-section in natural scale, while subplot b does the same in distorted scale in order to highlight its details. Hence, subplot b also includes an idealization of the ground surface, which shows that Ano Vathy sits roughly at the top of an (approximately triangular) valley with surface width $B = 300$ m and maximum thickness $H = 40$ m at the location where the probable or covered geological fault (with a NNW-SSE direction) lies (see also Fig. 28) at the western side of Ano Vathy. This western side of Ano Vathy exhibits the steepest bedrock inclination ($i = 28°$) and tallest outcropping bedrock (73 m with $i = 18°$), whereas at the eastern side the bedrock inclination is milder ($i = 14°$) and the outcropping bedrock is quite shorter (30 m with $i = 7°$).

In this cross-section, (ground surface) topography effects alone give negligible amplification at Ano Vathy, since it lies at the base of the canyon-shaped topography where seismic strong motion is generally not significantly amplified (Papadimitriou 2019). However, the valley-shaped stratigraphy of the underlying layers may be considered a cause of increased seismic ground motion at Ano Vathy, concurrently with that due to surface topography effects that was depicted along the NW–SE direction (see Fig. 29). It may be

Fig. 30 Ground surface elevation and approximate geological cross section along the SW-NE section running through the damaged area of Ano Vathy. Average (idealized) width of valley is 300 m
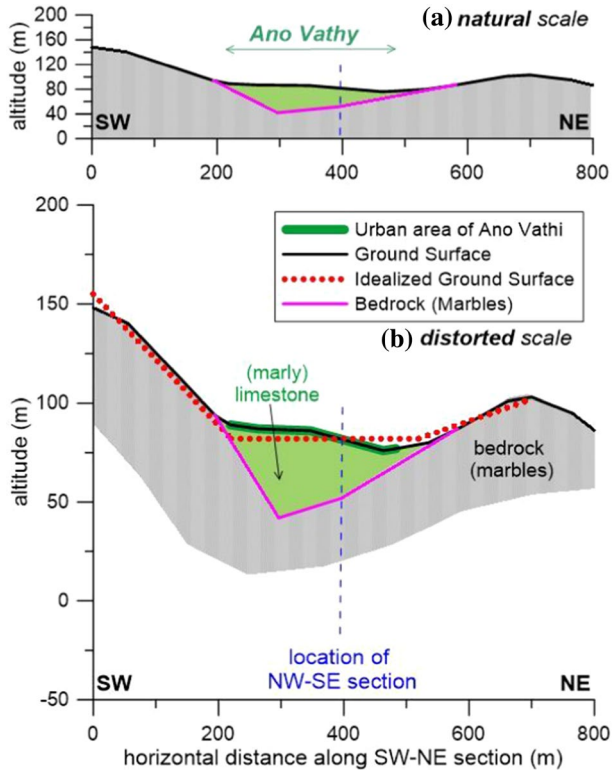
assumed here that the role of "soft" soil should be attributed to the marly limestone with a $V_s > 500$ m/s, that overlies the bedrock (marbles with $V_s > 800$ m/s), and consequently this valley-shaped structure is not expected to have an intense impedance contrast. In other words, this is not a typical alluvial valley with an intense soil–bedrock impedance contrast. However, the geomorphology shown in Fig. 30 allows for the generation of surface waves within the "softer" (marly) bedrock that locally amplify strong ground motion. Unfortunately, there are no code provisions for valley effects on seismic ground motion and any approximate estimation may only be based on the literature. For example, according to Vessia et al. (2011), this valley has a thickness over half-width shape ratio SR = 40/(300/2) = 0.27 (intermediate-depth valley), leading to an amplification of at least 35%, on top of ordinary 1D soil amplification. In this case, this value should be considered an upper limit since the valley material is not soft alluvium and the horizontal acceleration has a low-frequency content (predominant period 0.5 s), thus increasing the predominant shear wavelength to values comparable with the valley width and much larger than the valley thickness (Papadimitriou 2019). However, the aforementioned 35% amplification may be considered an appropriate value if one also considers any 1D soil amplification (Ground Category B as per EC8), as well as the enhanced amplification effect due to the outcropping bedrock slopes (Papadimitriou 2019). This is especially true at its western side where the bedrock slopes are relatively tall (73 m). In addition, this valley configuration may have also created parasitic vertical acceleration due to refractions of incident waves at the non-horizontal valley edges and the related surface wave generation. As in the case of slopes,

the term "parasitic" again implies that this component is independent of the incident vertical acceleration of the earthquake and appears primarily within the valley. In this case, the valley configuration may have also created low frequency (predominant period 0.5 s) parasitic vertical accelerations, whose intensity should be in the order of 10% of the peak horizontal acceleration (Papadimitriou et al. 2018). This parasitic vertical acceleration is also disregarded by EC8.

Hence, overall, Ano Vathy seems to lie at an unfavorable location in terms of its ground surface topography and its bedrock geomorphology. This must have led to coupled topography-valley amplification phenomena and a possible amplification (over the outcropping bedrock motion) in the order of 45% in the horizontal acceleration ($\approx 1.08 \times 1.35$) at the western side of Ano Vathy and less so (e.g., 1.25) at its eastern side. These horizontal amplifications apply to the short period components of the horizontal acceleration (for structural periods up to 0.5 s) and diminish for larger periods (e.g., for structural periods larger than 1 s; Papadimitriou 2019). In addition, this geomorphology must have created low frequency (predominant period 0.5 s) parasitic vertical acceleration (in the order of 20% of the horizontal component), which adds to the high frequency (predominant period 0.1 s) vertical acceleration of the bedrock motion itself. These coupled amplification effects may explain, partly at least, the increased structural damage observed at Ano Vathy during the October 30th 2020 earthquake.

4 Major findings and conclusions

The Samos (Aegean Sea) earthquake is noteworthy to discuss due to relatively more concentrated structural damage in Izmir Bayrakli and Samos-Vathy regions. In addition to poor structural design, detailing and construction practices, site effects are observed to contribute to the level of observed structural damages. With reference to site effects in Izmir Bay, the amplifying and prolonging effects of site conditions on seismic demand have been widely known and discussed in the geotechnical earthquake engineering literature. The response of the Mexico City basin subjected to the 1985 Mexico City Earthquake of $M_w = 8.1$ is a well-known case on how site effects can be the source of structural damage due to amplified and prolonged seismic demand. This event and the response of Izmir Bay has once again addressed the importance of these site effects. Followings are the major lessons learned from the earthquake:

(1) This event produced 2–3 standard deviation above median long period rock spectral acceleration intensities in the period range of 0.5–1.5 s, which is attributed to the slower source mechanism and the magnitude of the event.

(2) Deep soil sites of Izmir Bay, and more specifically Bayrakli, which have natural periods of 0.5–5 s, amplify further these already-relatively-long-period-rich rock excitations.

(3) Overlying 7–9 story reinforced concrete buildings, which happen to have natural periods also falling in this already amplified longer period range of 0.9–1.1 s resonated, which again further amplified the seismic demand.

(4) These double resonance effects (rock and soil resonance, and soil and superstructure resonance) amplified the overall response.

(5) Additionally, these site effects have also prolonged the seismic shaking duration.

(6) However, these amplified and prolonged excitations should not have triggered failure of structures since they are shown to be below design basis earthquake levels.

(7) There, poor structural design, detailing, and construction practices come into the picture.

(8) Code-based amplification factors for Izmir Bay and especially Bayrakli are shown to be exceeded by this relatively distant event and low-intensity seismic shaking. This clearly addresses the need to develop region-specific zonation, when general code practices are proven to be inadequate to assess such largely pronounced site effects.

With reference to site effects in Samos Island (greater Vathy area), the following are some preliminary findings:

(1) The event produced rather long period rock spectral accelerations on hard ground/ soft rock in the town of Vathy, in the period range 0.4—0.6 s and significant durations of up to 9 s. This, again, can be attributed to the size of the rupture.

(2) Although located only about 10 km from the rupture (22 km from the epicenter), within the near-fault zone, the town of Vathy was rather lightly affected by the earthquake, with relatively few collapsed or heavily damaged buildings. This can be partially attributed to the low height / low weight of structures in the area.

(3) The strong ground motion recordings on stiff sites close to shore in the town of Vathy had relatively modest horizontal PGA and PGV values, of up to 0.23 g and 22 cm/s, respectively. Moreover, one may consider the ITSAK and NOA recording sites as being a "stiff soil" ($V_{s,30} = 550$ m/s) and a "bedrock" site ($V_{s,30} = 840$ m/s), respectively. On the basis of this approximation, 1D soil amplification is found to be significant within the town of Vathy, i.e., on the order of 30% on average.

(4) Concentration of damage in low-rise buildings in the old town of Vathy (Ano Vathy hill), at a distance of 600–1000 m from shore and an elevation of 50–120 m (having an approximate area of 0.1 km^2), is indicative of a combination of coupled valley and topography phenomena. Such effects have been observed in other recent earthquakes in Greece (e.g., Margaris et al. 2008, Nikolaou et al. 2014)

(5) Ano Vathy seems to lie at an unfavorable location in terms of its ground surface topography and bedrock geomorphology. This combination may have led to a possible amplification of the horizontal acceleration (over that of the outcropping bedrock motion) in the order of 25–45%, especially for low structural periods.

(6) In addition, the geomorphology of Ano Vathy may have created low frequency (predominant period 0.5 s) parasitic vertical acceleration (in the order of 20% of the horizontal component), which adds to the high frequency (predominant period 0.1 s) vertical acceleration of the bedrock motion itself (e.g., as recorded at NOA site).

The above findings for Vathy town indicate a long-period bedrock motion that is rather uncommon for the earthquake regime of Greece. More importantly, they show significant 1D soil amplifications in stiff soil conditions (Ground Category B of EC8) that surpass the EC8-prescribed amplification of 1.2 for periods up to TB = 0.4 s. Concurrently, the EC8 provisions for an amplification of 1.5 seem quite conservative for large periods (larger than 1.0 s). In addition, the above findings for Ano Vathy stress the importance of surface topography and bedrock geomorphology for altering the characteristics of seismic ground motion. Their combined (2D or even 3D) effects prove as important as those of 1D soil amplification, yet only for low periods (up to 1.0 s), which, however, are the most important periods for ordinary structures covered by code provisions. Nevertheless, these effects are yet to be considered in a systematic manner by the EC8. In closing, the site effects in

Samos Island during this earthquake prove a significant case-study for shaping future editions of the EC8, or any other seismic code worldwide.

Moreover, as the most important concluding remark, on the basis of reconnaissance findings from both Turkish and Greek sites, site effects (including site profile-, surface and subsurface topographical-effects) were acknowledged as the most pronounced factor, which govern the overall seismic demand and observed corollary structural damage. These amplifications due to site effects were either not addressed at all, or exceed the factors suggested by national design codes, recommending the need to re-visit them, as they were proven to be inadequate to assess the extreme site effects observed in Bayrakli-Izmir and Ano Vathy hills-Samos.

References

Abrahamson N, Silva WJ, Kamai R (2014) Summary of the ASK14 Ground Motion Relation for Active Crustal Regions. Earthq Spectra 30(3):1025–1055. https://doi.org/10.1193/070913EQS198M

Akbuga E (2019) Seferihisar (Izmir) Bolgesinde Sivilasma Analizi ve Haritalandirilmasi. Manisa Celal Bayar Üniversitesi, Master Thesis (in Turkish)

Boore DM, Stewart JP, Seyhan E, Atkinson GM (2014) NGA-West2 equations for predicting PGA, PGV, and 5% damped PSA for shallow crustal earthquakes. Earthq Spectra 30:1057–1085

Bouckovalas GD, Papadimitriou AG (2005) Numerical evaluation of slope topography effects on seismic ground motion. Soil Dyn Earthq Eng 25(7–10):547–555

Building Seismic Safety Council (BSSC) (2020) NEHRP Recommended Seismic Provisions for New Buildings and Other Structures, FEMA P-2082–1, Washington, DC, pp 593. https://www.fema.gov/sites/default/files/2020-10/fema_2020-nehrp-provisions_part-1-and-part-2.pdf

Campbell KW, Bozorgnia Y (2014) NGA-West2 ground motion model for the average horizontal components of PGA, PGV, and 5% damped linear acceleration response spectra. Earthq Spectra 30:1087–1115

Cetin KO, Altun S, Askan A, Akgün M, Sezer A, Kıncal C, Ozdag OC, Ipek Y, Unutmaz B, Gulerce Z, Ozacar AA, Ilgaç M, Can G, Cakir E, Söylemez B, El-Sayeed A, Zarzour M, Bozyiğit I, Tuna C, Köksal D, Karimzadeh S, Uzel B, Karaali E (2021) The site effects in Izmir Bay of October 30 2020, M7.0 Samos Earthquake. Soil Dyn Earthq Eng (under review)

Chiou BSJ, Youngs RR (2014) Update of the Chiou and Youngs NGA model for the average horizontal component of peak ground motion and response spectra. Earthq Spectra 517(30):1117–1153

EN 1998-1 (2004) Eurocode 8: design of structures for earthquake resistance. 1st ed, Brussels, BSi

Erdoğan B (1990) Stratigraphy and tectonic evolution of İzmir-Ankara zone between İzmir and Seferihisar. TAPG Bull 2(1):1–20 (**in Turkish**))

Gulerce Z, Akbaş B, Özacar AA, Sopacı E, Önder FM, Uzel B, Can G, Cakir E, Ilgaç M, Söylemez B, Saltoğlu N, Askan A, Cetin KO, Unutmaz B. (2021) Predictive performance of current ground motion models for recorded strong motions in 2020 Samos Earthquake. Soil Dyn Earthq Eng (under review)

HSGME (Hellenic Survey of Geology and Mineral Exploration) (1979) Geological Map of Samos Island (Scale 1:50,000).

ITSAK- EPPO (2020) The Earthquake of Oct. 30, 2020, Mw7.0 (11:51GMT) North of Samos Island (Greece): Observed strong ground motion on Samos island, -Preliminary Report ITSAK v3.0, Thessaloniki p 9

Kalogeras I, Melis NS, Kalligeris N (2020) The earthquake of October 30th, 2020, at Samos, Eastern Aegean Sea, Greece. Preliminary Report v2., National Observatory of Athens, Institute of Geodynamics, Greece

Kıncal C (2005) Engineering geological evaluation of geological units outcrop in and around the Izmir city centre with the help of geographical information systems and remote sensing techniques, Dokuz Eylul University, The Graduate School of Natural and Applied Sciences, PhD thesis, p 342, Izmir (in Turkish).

Koca, M. Y. (1995) Slope stability assessment of the abandoned andesite quarries in and around the Izmir city centre. Unpublished Ph.D. thesis, Dokuz Eylul University, Izmir, p 430

Kubilay K (2012) Deprem Dalgalarinin Zemin Büyütmesi Üzerine Örnekler. TÜBAV Bilim Dergisi 5(4):17–32

Margaris V, Papaioannou C, Theodoulidis N, Savvaidis A, Klimis N, Makra K, Karakostas C, Lekidis V, Makarios T, Salonikios T, Demosthenus M, Athanasopoulos G, Mylonakis G, Papantonopoulos C, Efthymiadou V, Kloukinas P, Ordonez I, Vlachakis V, and Stewart JP (2008) Preliminary report on the principal seismological and engineering aspects of the Mw = 6.5 Achaia-Ilia (Greece) earthquake on 8 June 2008. GEER Association Report No. GEER-013, Web report

Mayoral J, Asimaki D, Tepalcapa S, Wood C, Roman-de la Sancha A, Hutchinson T et al (2019) Site effects in Mexico City basin: Past and present. Soil Dyn Earthq Eng 121:369–382. https://doi.org/10.1016/j.soildyn.2019.02.028

Nikolaou et al (2014) Geotechnical Aspects of the M = 6.1 January 27 and February 03, 2014, Cephalonia, Greece, Earthquakes. GEER Association Report No. GEER-034 Web report

Pamuk E, Akgün M, Özdağ Ö, Gönenç T (2017) 2D soil and engineering-seismic bed-rock modeling of eastern part of Izmir inner bay/Turkey. J Appl Geophys 137:104–117. https://doi.org/10.1016/j.jappgeo.2016.12.016

Pamuk E, Gönenç T, Özdağ ÖC et al (2018a) 3D Bedrock Structure of Bornova Plain and Its surroundings (İzmir/Western Turkey). Pure Appl Geophys 175:325–340. https://doi.org/10.1007/s00024-017-1681-0

Pamuk E, Özdağ ÖC, Akgün M (2018b) Soil characterization of Bornova Plain (Izmir, Turkey) and its surroundings using a combined survey of MASW and ReMi methods and Nakamura's (HVSR) technique. Bull Eng Geol Environ 78:3023–3035. https://doi.org/10.1007/s10064-018-1293-7

Pamuk E, Özdağ ÖC, Akgün M (2019) Soil characterization of Bornova Plain (Izmir, Turkey) and its surroundings using a combined survey of MASW and ReMi methods and Nakamura's (HVSR) technique. Bull Eng Geol Env 78(4):3023–3035

Papadimitriou AG (2019) An engineering perspective on topography and valley effects on seismic ground motion. Theme Lecture, 7th International Conference on Earthquake Geotechnical Engineering, June 16–19, Rome, Italy

Papadimitriou AG, Paraskevopoulos SA, and Lamprakopoulos AN (2018) Aggravation of spectral acceleration along 2D symmetrical trapezoidal valleys. Proceedings, 16th European Conference on Earthquake Engineering, Thessaloniki, Greece, Paper ID: 11491

Roche V, Jolivet L, Papanikolaou D, Bozkurtf E, Menant A, Rimmelé G (2019) Slab fragmentation beneath the Aegean/Anatolia transition zone: Insights from the tectonic and metamorphic evolution of the Eastern Aegean region. Tectonophysics 754:101–129

Rollins KM, Singh M, Roy J (2020) Simplified Equations for Shear-Modulus Degradation and Damping of Gravels. J Geotech Geoenviron Eng 146(9):1. https://doi.org/10.1061/(ASCE)GT.1943/5606.0002300

Schnabel PB (1973) Effects of local geology and distance from source on earthquake ground motions. PhD Thesis, University of California, Berkeley, California

Seed HB, Idriss IM (1970) Soil moduli and damping factors for dynamic analysis. EERC Report No. 10–70, University of California

Stewart JP, Klimis N, Savvaidis A, Theodoulidis N, Zargli E, Athanasopoulos G, Pelekis P, Mylonakis G, Margaris B (2014) Compilation of a local vs profile database and its application for inference of VS30 from geologic- and terrain-based proxies. Bull Seism Soc Am 104(6):2827–2841

TEC (2018). Turkish Earthquake Code: Specifications for Building Design Under Earthquake Effects

Vessia G, Russo S, Lo Presti D (2011) A new proposal for the evaluation of the amplification coefficient due to valley effects in the simplified local seismic response analyses. Rivista Italiana Di Geotecnica 4:51–77

Vucetic M, Dobry R (1991) Effect of Soil Plasticity on Cyclic Response. J Geotech Eng 117:89–107

Yakut A, Binici B, Ilki A, Canbay E, Donmez C (2021) Observations, Damage distribution and Performance of Buildings in İzmir after the Samos Island Earthquake. Bull Earthq Eng (under review)

Authors and Affiliations

Kemal Onder Cetin[1] [iD] **· Achilleas G. Papadimitriou[2] · Selim Altun[3] · Panagiotis Pelekis[4] · Berna Unutmaz[5] · Emmanouil Rovithis[6] · Mustafa Akgun[7] · Nikolaos Klimis[8] · Aysegul Askan[1] · Katerina Ziotopoulou[9] · Alper Sezer[3] · Cem Kincal[7] · Makbule Ilgac[1] · Gizem Can[1] · Elife Cakir[1] · Berkan Soylemez[1] · Ahmed Al-Suhaily[1] · Alaa Elsaid[1] · Moutasem Zarzour[1] · Jonathan Stewart[10] · George Mylonakis[10,11,12]**

✉ Kemal Onder Cetin
ocetin@metu.edu.tr

[1] Middle East Technical University, Universiteler Mah, Dumlupınar Bulv, 06800 Cankaya-Ankara, Turkey

[2] National Technical University of Athens, Athens, Greece

[3] Ege University, Izmir, Turkey

[4] University of Patras, Patras, Greece

[5] Hacettepe University, Ankara, Turkey

[6] Institute of Engineering Seismology and Earthquake Engineering, Thessaloniki, Greece

[7] Dokuz Eylül University, Izmir, Turkey

[8] Democritus University of Thrace, Komotiny, Greece

[9] University of California Davis, Davis, USA

[10] University of California, Los Angeles, USA

[11] Khalifa University, Abu Dhabi, UAE

[12] University of Bristol, Bristol, UK